AGU PUBLICATIONS

JGR

Journal of Geophysical Research: Solid Earth

RESEARCH ARTICLE
10.1002/2015JB011952

Key Points:
- A study of magnetic mineral diagenesis in river-dominated coastal margins
- Higher sedimentation rates lead to a deeper zone of rapid magnetite dissolution
- Magnetic methods provide a tool for assessing iron-sulfur relationships

Correspondence to:
W. Zhang,
wgzhang@sklec.ecnu.edu.cn

Citation:
Ge, C., W. Zhang, C. Dong, Y. Dong, X. Bai, J. Liu, N. T. T. Hien, H. Feng, and L. Yu (2015), Magnetic mineral diagenesis in the river-dominated inner shelf of the East China Sea, China, *J. Geophys. Res. Solid Earth*, *120*, 4720–4733, doi:10.1002/2015JB011952.

Received 17 FEB 2015
Accepted 7 JUN 2015
Accepted article online 10 JUN 2015
Published online 29 JUL 2015

Magnetic mineral diagenesis in the river-dominated inner shelf of the East China Sea, China

Can Ge[1], Weiguo Zhang[1], Chenyin Dong[1,2], Yan Dong[3], Xuexin Bai[1], Jinyan Liu[1], Nguyen Thi Thu Hien[1], Huan Feng[4], and Lizhong Yu[1]

[1]State Key Laboratory of Estuarine and Coastal Research, East China Normal University, Shanghai, China, [2]Now at Department of Environmental Sciences, Faculty of Science and Engineering, Macquarie University, Sydney, New South Wales, Australia, [3]Institute of Geographic Engineering Technology, School of Geographical Science, Nantong University, Nantong, China, [4]Department of Earth and Environmental Studies, Montclair State University, Montclair, New Jersey, USA

Abstract The inner shelf of the East China Sea is a river-dominated margin characterized by fine-grained mud deposits and a rapid sedimentation rate. Three short sediment cores (~2.7 m in length) were examined to characterize spatial variations in magnetic mineral diagenesis. The sediment cores were analyzed for sedimentation rates, magnetic properties, particle size distribution, organic carbon, and total sulfur content. The two more proximal cores with higher sedimentation rates (~2.2 cm/yr and ~0.96 cm/yr) do not exhibit obvious effects of reductive dissolution of magnetite with increasing depth, which is consistent with their lower total sulfur content. The offshore core, A12-4, which has a lower sedimentation rate, contains clear evidence of magnetite dissolution and increasing total sulfur content with depth. The three cores have a similar sediment source and organic matter input; therefore, we suggest that a higher sedimentation rate will lead to less reductive diagenesis of magnetite, assuming that other factors are constant. The iron- to sulfate-reduction boundary, i.e., revealed by the onset of a rapid decline of magnetic susceptibility, is located 1.0 m below seafloor in core A12-4. This is much deeper than is reported in many other coastal marine environments and can be explained by the higher sedimentation rate, the presence of refractory terrestrial organic matter, and an abundant input of detrital iron oxides. This study demonstrates that analyses of the magnetic mineral zonation provide a straightforward approach to assess diagenetic organic carbon decomposition pathways in marine environments.

1. Introduction

The influence of reductive diagenesis on magnetic properties is well documented in marine environments [*Karlin and Levi*, 1983; *Canfield and Berner*, 1987; *Bloemendal et al.*, 1992; *Kawamura et al.*, 2007; *Fu et al.*, 2008; *Rowan et al.*, 2009; *Mohamed et al.*, 2011; *Bouilloux et al.*, 2013; *Roberts et al.*, 2013]. Driven by organic matter degradation, electron acceptors such as iron oxides and sulfate are reduced and a variety of iron-containing minerals are either destroyed or formed, which has a profound impact on sediment magnetism. Normally, the process is characterized by a declining trend of ferrimagnetic mineral (e.g., magnetite) concentration with increasing depth [*Karlin and Levi*, 1983]. In association with the decrease in magnetite concentration, there is a change in the grain size distribution of magnetite, with fine grains removed followed by the breakdown of coarser grains [*Karlin*, 1990; *Bloemendal et al.*, 1992; *Robinson et al.*, 2000]. Since imperfect antiferromagnetic minerals, such as hematite and goethite, are more resistant to reductive dissolution compared to magnetite [*Yamazaki et al.*, 2003; *Emiroğlu et al.*, 2004; *Liu et al.*, 2004; *Rey et al.*, 2005; *Kawamura et al.*, 2007; *Rowan et al.*, 2009; *Mohamed et al.*, 2011], there will be a relative increase in the proportion of imperfect antiferromagnetic minerals with depth, which can be reflected by variations of the *S* ratio [*Robinson et al.*, 2000]. Paramagnetic iron sulfides (e.g., pyrite), or carbonates (e.g., siderite), are typical products of reductive diagenesis [*Burdige*, 1993]. Greigite, an intermediate product during pyrite formation, may also occur [*Tric et al.*, 1991; *Horng et al.*, 1992; *Roberts and Turner*, 1993], which can lead to a more complicated stratigraphic variation of magnetic properties [*Fu et al.*, 2008; *Blanchet et al.*, 2009]. The onset of the rapid decline of ferrimagnetic mineral concentration occurs at the boundary between the iron- and sulfate-reduction diagenetic zones [e.g., *Rowan et al.*, 2009; *Mohamed et al.*, 2011; *Zheng et al.*, 2011].

In continental margins influenced by large rivers (i.e., river-dominated margins), the sediment accumulation rate is generally high due to the abundant fluvial delivery of sediments. Thus, continental margins are

important areas for studying the global carbon cycle since they are loci for terrestrial carbon burial as well as for carbon production and remineralization [*Blair and Aller*, 2012]. Normally, carbon burial efficiency in marine environments increases with sediment accumulation rate [*Hedges and Keil*, 1995; *Burdige*, 2005]. However, carbon burial efficiency in some river-dominated margins is lower than expected [*Burdige*, 2005]. Efficient oxidation of organic carbon in highly dynamic fluid muds has been suggested to be the main cause of the poor preservation of organic carbon in such environments [*Blair and Aller*, 2012]. Therefore, it is anticipated that the nature of magnetic mineral diagenesis in such environments will differ significantly from that of pelagic marine sediments.

The East China Sea is a typical river-dominated marginal sea due to abundant sediment input from the Yangtze River [*Liu et al*., 2007]. As a result, recent sediment deposition rates in the inner shelf can reach several centimeters per year [*DeMaster et al*., 1985; *Huh and Su*, 1999]. Compared to other marine environments, studies of magnetic mineral diagenesis in recent sediments of river-dominated margins are still limited. *Zheng et al*. [2011] documented the occurrence of magnetic mineral diagenesis in Holocene deposits from the inner shelf of the East China Sea, where the average sedimentation rate can be 2–4 mm/yr (2 to 4 m/kyr) on a millennial time scale. They found that the iron- to sulfate-reduction boundary (ISRB) is located at a depth of 1.1 m (in core MD06-3042) below the seafloor, which is deeper than in some normal marine environments and in highly biologically productive sediment-poor coastal areas such as the Ria de Vigo, northwestern Iberian Peninsula (e.g., several centimeters to tens of centimeters) [*Mohamed et al*., 2011].

The combination of intensive land-ocean interaction and shallow water in coastal areas results in a high degree of spatial variability in sedimentary and biogeochemical processes. This has been clearly demonstrated in the Ria de Vigo, northwestern Iberian Peninsula, which reveal a steep gradient in magnetic mineral diagenesis in a transect from the inner estuary to offshore environments [*Mohamed et al*., 2011]. In the present study, we examined the magnetic properties of three short cores (~2.7 m) along a short transect in the inner shelf of the East China Sea (Figure 1). Given the similarity of sediment source and depositional environment of the core sites, the purpose of the study is to investigate how organic matter content and sedimentation rate affect magnetic mineral diagenesis in this river-dominated coastal environment with rapid sediment accumulation rate. The aim was to obtain improved insights into the origin of contrasts in magnetic mineral diagenesis in different near-shore marine environments.

2. Study Area and Methods

In the inner shelf (~50 m water depth) of the East China Sea, a belt of muddy sediments extends from the Yangtze River Estuary southward to the northern section of the Taiwan Strait (Figure 1) [*Qin et al*., 1987]. Coastal currents include the northward flowing Taiwan Warm Current and the Zhejiang-Fujian (Zhe-Min) Coastal Current, which flows southward in winter and northward in summer (Figure 1). Approximately one half of the fluvial sediment load of the Yangtze River exits the Yangtze Estuary and is delivered to the East China Sea [*Milliman et al*., 1985]. Due to the dominant southward flowing long-shore currents in winter, sediments from the Yangtze River are transported southward along the coast and are deposited in the inner shelf of the East China Sea. Mud deposits occur as a clinoform along the coast, which dips at around a water depth of ~50 m [*Liu et al*., 2007]. This mud zone is dominated by clayey silts; modern sedimentation rates in the northern section of the mud belt are high, ranging from 0.8 to 2 cm/yr [*Huh and Su*, 1999].

Our study area is located in the northern part of the coastal mud zone along the Zhejiang-Fujian coast. Three gravity cores along a transect perpendicular to the coast, namely, cores A12-1 (29°15′28″N, 122°19′12″E), A12-2 (29°13′22″N, 122°24′06″E), and A12-4 (29°08′27″N, 122°33′55″E), were retrieved in March 2013 from water depths of 21.5 m, 31.0 m, and 51.0 m, respectively (Figure 1). The cores are composed mainly of clayey silts, which change from a brownish to a grayish color with increasing depth.

Each core was sampled at 2 cm stratigraphic intervals. All samples were dried at low temperature (<40°C) before undertaking magnetic analyses. Magnetic susceptibility was measured using a Bartington Instruments MS2B magnetic susceptibility meter at low (0.47 kHz) and high (4.7 kHz) frequencies (χ_{lf} and χ_{hf}, respectively). Frequency-dependent susceptibility (χ_{fd}) was calculated as the difference between χ_{lf} and χ_{hf} (i.e., $\chi_{fd} = \chi_{lf} - \chi_{hf}$) and is expressed in mass-specific terms. An anhysteretic remanent magnetization (ARM)

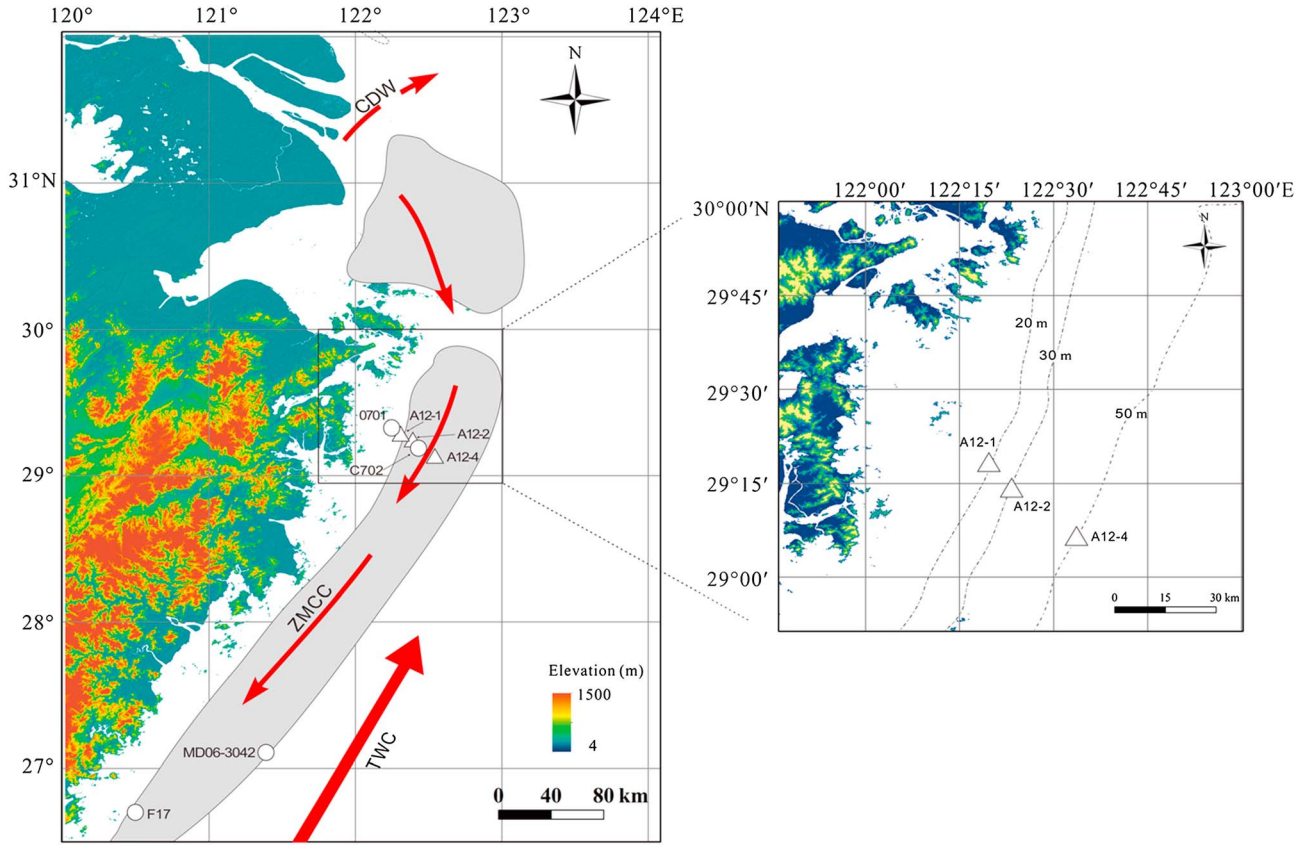

Figure 1. Study area and locations of cores A12-1, A12-2, and A12-4, together with locations of additional cores referenced in the text: C702 [*Zhu et al.*, 2013], F17 [*Hu et al.*, 2012], MD06-3042 [*Zheng et al.*, 2011], and 0701 [*Lü et al.*, 2011]. The shaded zone represents the zone of accumulation of muddy sediments (modified after *Qin et al.* [1987]). Currents in the study area are also shown, including the Changjiang Diluted Water (CDW), the Zhe-Min Coastal Current (ZMCC), and the Taiwan Warm Current (TWC).

was imparted in a 0.04 mT direct current (DC) bias field that was superimposed on a peak alternating field (AF) of 100 mT using a DTECH 2000 AF demagnetizer and was measured using a Molspin magnetometer. ARM is expressed as an anhysteretic susceptibility (χ_{ARM}) by normalizing ARM by the applied DC field. Isothermal remanent magnetization (IRM) measurements were made using a forward field of 1 T followed by application of backfields of −100 mT and −300 mT that were imparted using an MMPM10 pulse magnetizer. The IRM imparted with a 1 T induction is referred to as a "saturation" IRM (SIRM), and the backfield remanence is referred to as $IRM_{x\ mT}$, where x mT denotes the backfield value. Hard IRM was calculated as $HIRM = 0.5 \times (SIRM + IRM_{300\ mT})$. S ratios (S_{-100} and S_{-300}) were calculated as $S_{-100} = 100 \times (SIRM - IRM_{100\ mT})/(2 \times SIRM)$ and $S_{-300} = 100 \times (SIRM - IRM_{300\ mT})/(2 \times SIRM)$, respectively [*Bloemendal and Liu*, 2005].

Selected samples were used for stepwise IRM acquisition in 39 fields, ranging from 10 mT to 7.0 T. The field intervals were approximately equidistant on a log scale. Magnetic mineral assemblages were further investigated using IRM unmixing [*Kruiver et al.*, 2001]. Normally, the low-coercivity component refers to magnetite, while high-coercivity components are contributed by hematite or goethite [*Kruiver et al.*, 2001]. Finally, high-temperature thermomagnetic analysis was carried out using an MFK1-FA Kappabridge equipped with a CS-3 high-temperature furnace. Each sample was heated from room temperature to 700°C and was then cooled to room temperature in an argon atmosphere.

Bulk sediment particle size distributions were determined using a laser size analyzer (Coulter LS 13 320) with a measurement range of 0.04–2000 μm, following treatment with 5% H_2O_2 and 0.2 M HCl to remove organic matter and carbonate, respectively. Addition of 0.5 M $(NaPO_3)_6$ and ultrasonic dispersion were used to ensure complete particle disaggregation prior to analysis [*Lu*, 2000].

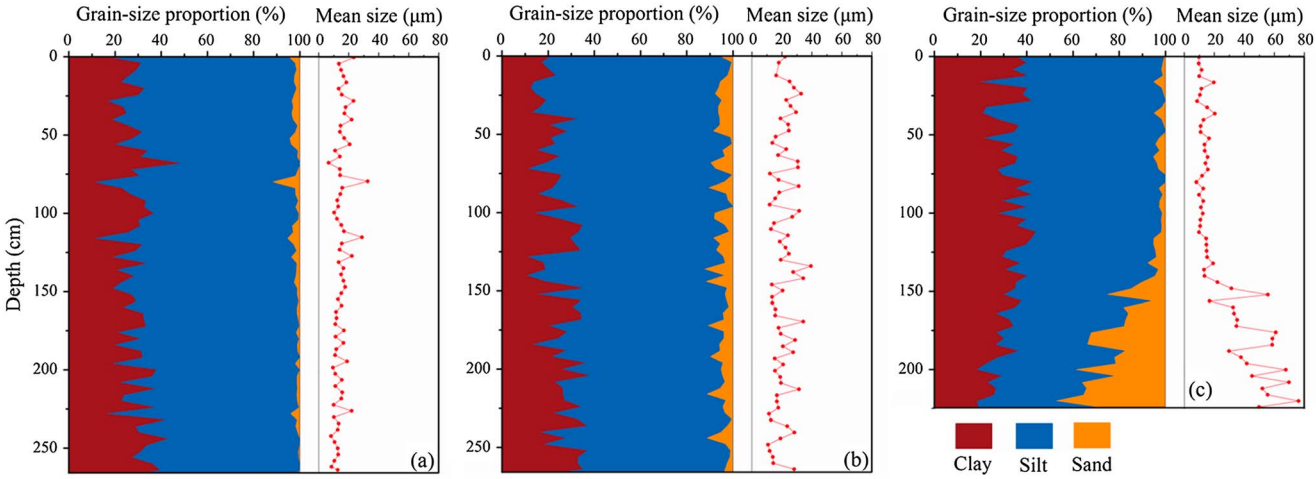

Figure 2. Downcore variations of sediment particle size composition and mean particle size for cores (a) A12-1, (b) A12-2, and (c) A12-4.

The ^{210}Pb and ^{137}Cs activities were measured in order to estimate the sedimentation rate [*Appleby and Oldfield*, 1978]. Sediment samples were sealed in holders for 3 weeks and were then counted using an HPGe γ spectrometer (GWL-120210S). Total ^{210}Pb and ^{214}Pb were determined from the gamma emissions at 46.5 keV and 351.9 keV, respectively, with the latter as the supported ^{210}Pb. Excess ^{210}Pb was calculated as the difference between total ^{210}Pb and ^{214}Pb. The ^{137}Cs was determined from the gamma emissions at 661 keV.

Selected samples (every 8 cm) were analyzed for total organic carbon (TOC) and total nitrogen (TN). TOC was analyzed using potassium-dichromate ($K_2Cr_2O_7$) titration [*Lu*, 2000]. TN was determined using a CHN analyzer (Vario EL III). The precision is better than 5%. For total sulfur (TS) analysis, selected samples (every 16 cm for cores A12-1 and A12-2 and every 8 cm for A12-4) were digested in a mixture of concentrated HNO_3-$HClO_4$ acids [*Shan et al*., 1991] and were analyzed by inductively coupled plasma–atomic emission spectrometry (Thermo iCAP 7400). The China National Reference Material GSD-9 was also included for quality control, with the reported TS value within 10% of the reference value.

3. Results

3.1. Particle Size Distribution

Cores A12-1 and A12-2 exhibit only minor variations in particle size distribution with depth (Figures 2a and 2b). Both are dominated by silt (4~63 μm), which ranges from 52.3 to 84.3% in the former and from 36.7 to 86.3% in the latter. The clay fraction ($<$4 μm) ranges from 10.1 to 47.7% in the former and from 8.8 to 42.1% in the latter. The sand fraction is a minor component in both cores (Figures 2a and 2b). In core A12-4, the particle size distribution is similar in the section above 150 cm, which has a mean grain size similar to those of cores A12-1 and A12-2 (Figure 2c). However, below 150 cm depth, the silt fraction decreases with depth, while the $>$63 μm fraction has the opposite trend.

3.2. Chronology

The irregular distribution and lack of excess ^{210}Pb in cores A12-1 and A12-2 preclude their use for dating (Figures 3a and 3b). This feature has also been found in the subaqueous delta of the Yangtze Estuary [*Chen et al*., 2004]. The ^{137}Cs activity peaks occur at depths of 110 cm, 48 cm, and 16 cm in cores A12-1, A12-2, and A12-4, respectively (Figures 3d–3f). If we assume that these peaks represent the year 1963, which corresponds to a peak in the atmospheric testing of nuclear weapons [*Huh and Su*, 1999; *Pan et al*., 2011], the ^{137}Cs profiles yield respective average sedimentation rates of 2.2 cm/yr, 0.96 cm/yr, and 0.32 cm/yr, respectively, for the layers above the peaks. In addition, these values are supported by estimates based on an excess ^{210}Pb profile using the constant initial concentration model [*Appleby and Oldfield*, 1978] from the upper 30 cm of sediment in core A12-4, which yields a mean sedimentation rate of ~0.37 cm/yr (Figure 3c). The observed pattern of sedimentation rates decreasing eastward from

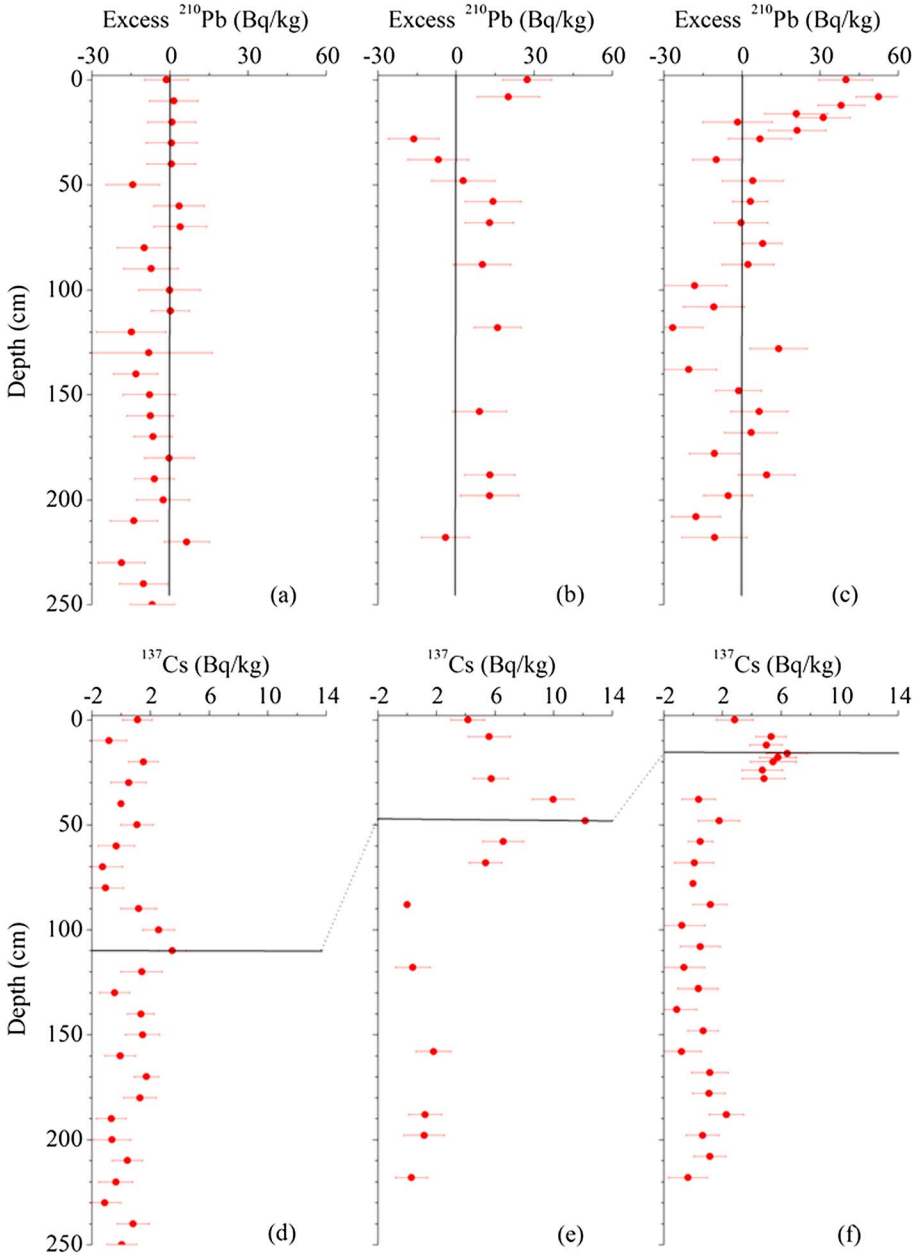

Figure 3. Downcore variations of excess ^{210}Pb activity for cores (a) A12-1, (b) A12-2, and (c) A12-4. (d–f) The corresponding ^{137}Cs activity, respectively. The horizontal lines denote a peak in ^{137}Cs activity, which is assumed to correspond to the 1963 maximum in atmospheric testing of nuclear weapons [*Huh and Su*, 1999].

onshore to offshore is similar to the results of a study in the adjacent area, which reported rates ranging from ~2 cm/yr to <0.1 cm/yr [*Huh and Su*, 1999].

3.3. Magnetic Properties

3.3.1. Bulk Magnetic Properties

Parameter χ and SIRM generally reflect the concentration of magnetic minerals, especially ferrimagnetic minerals (e.g., magnetite) [*Thompson and Oldfield*, 1986; *Liu et al*., 2012]. Unlike SIRM, χ is also influenced by paramagnetic and diamagnetic minerals [*Thompson and Oldfield*, 1986]. Parameter χ_{ARM} is particularly sensitive to single-domain (SD) ferrimagnetic grains [*Maher*, 1988]. Parameter χ_{fd} reflects the presence of fine viscous grains close to the superparamagnetic (SP)/SD boundary [*Thompson and Oldfield*, 1986;

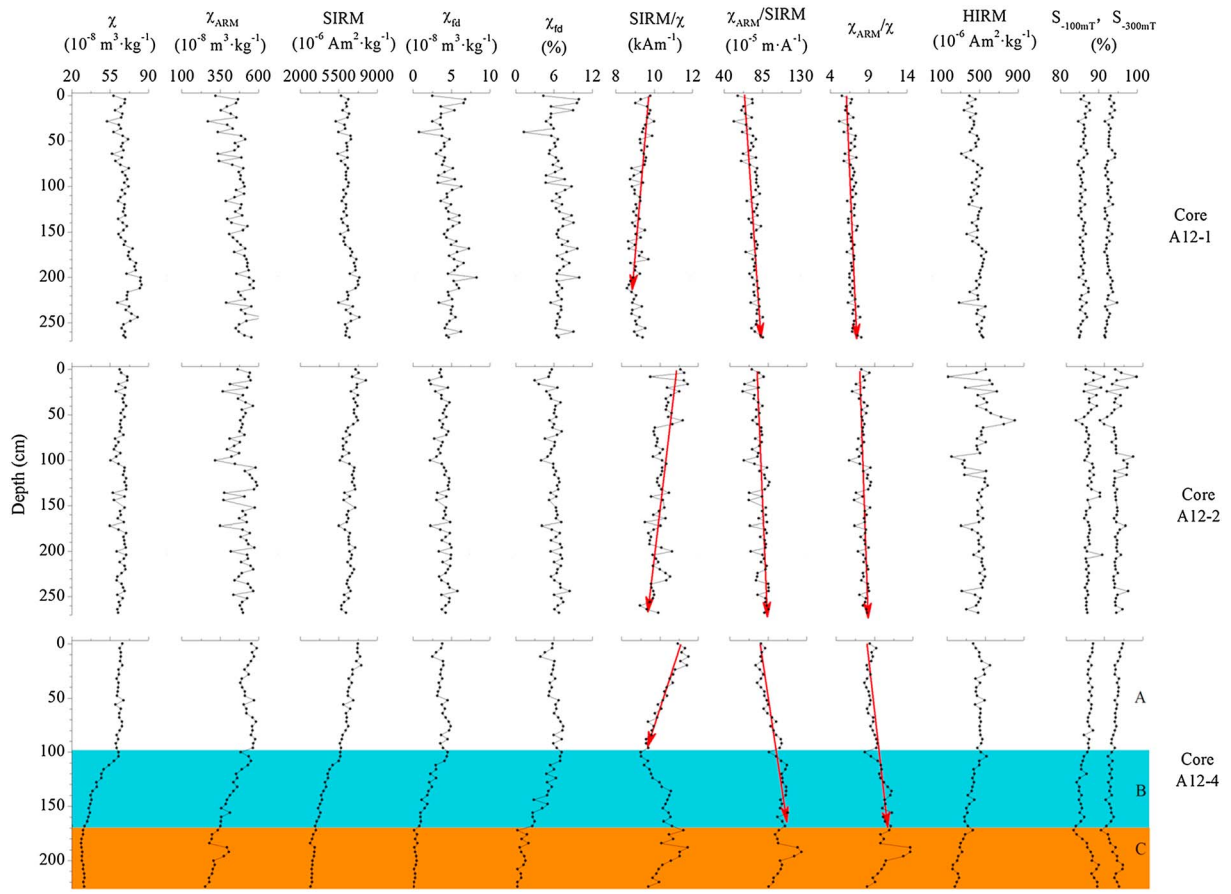

Figure 4. Downcore variations of magnetic properties for cores A12-1, A12-2, and A12-4.

Liu et al., 2012]. HIRM is commonly used to estimate the concentration of high-coercivity minerals (e.g., hematite and goethite). In cores A12-1 and A12-2, χ and SIRM exhibit similar trends with minor variability, implying that χ is dominated by ferrimagnetic minerals (Figure 4). Parameter χ_{ARM} and HIRM increase slightly with depth in core A12-1 and exhibit no obvious trend in core A12-2. Parameter χ_{fd} is higher in the upper 20 cm of core A12-1. It increases slightly with depth until 200 cm, after which it decreases with depth. In core A12-2, χ_{fd} increases gradually with depth.

Parameter χ_{ARM}/SIRM is commonly used as a grain size indicator for ferrimagnetic minerals, peaking in the SD range and decreasing with increasing grain size [*Maher*, 1988]. Parameter χ_{ARM}/χ has also been proposed as a grain size indicator [*Banerjee et al.*, 1981]; however, its relationship to ferrimagnetic grain size depends on whether the grain assemblages are mainly larger or smaller than SD size [*Oldfield*, 1994]. The contribution of paramagnetic mineral to χ can complicate the interpretation of χ_{ARM}/χ as a grain size indicator. SIRM/χ can be influenced by a number of factors, and a higher proportion of high coercivity minerals can lead to higher values [*Thompson and Oldfield*, 1986]. S_{-300} serves as a measure of the relative importance of low- (e.g., magnetite and maghemite) and high- (e.g., hematite and goethite) coercivity components in the total magnetic mineral assemblage [*Bloemendal and Liu*, 2005], while S_{-100} reflects the ratio of low-coercivity minerals to medium- and high-coercivity minerals [*Yamazaki*, 2009; *Yamazaki and Ikehara*, 2012]. In both cores (Figure 4), χ_{ARM}/SIRM and χ_{ARM}/χ exhibit a slightly increasing trend with depth, while SIRM/χ exhibits the opposite trend. S_{-100} and S_{-300} are uniform in both cores. Parameter $\chi_{fd\%}$ variations follow those of χ_{fd} in each core, fluctuating slightly around 6%.

In core A12-4 (Figure 4), χ, χ_{ARM}, χ_{fd}, and HIRM remain relatively stable in the upper 100 cm (Zone A), with values similar to those of cores A12-1 and A12-2 (Table 1). Beginning at 100 cm, they exhibit a decreasing

Table 1. Summary of Magnetic, Geochemical, and Bulk Sediment Particle Size Analyses for Cores A12-1 and A12-2 and for the Upper 100 cm of Core A12-4

	A12-1			A12-2			A12-4 (0–100 cm)		
	Minimum	Maximum	Mean ± SD	Minimum	Maximum	Mean ± SD	Minimum	Maximum	Mean ± SD
χ (10^{-8} m^3 kg^{-1})	52	84	69 ± 6	55	71	65 ± 4	60	67	63 ± 2
SIRM (10^{-6} Am^2 kg^{-1})	5240	7397	6295 ± 461	5493	7968	6549 ± 476	5608	7556	6491 ± 572
χ_{fd} (10^{-8} m^3 kg^{-1})	0.74	8.25	4.69 ± 1.20	2.09	5.79	3.98 ± 0.74	2.51	4.91	3.83 ± 0.57
χ_{ARM} (10^{-8} m^3 kg^{-1})	270	633	467 ± 65	316	590	493 ± 60	482	589	539 ± 33
HIRM (10^{-6} Am^2 kg^{-1})	286	569	462 ± 58	109	807	441 ± 111	373	548	444 ± 37
χ_{ARM}/SIRM (10^{-5} m A^{-1})	51	86	74 ± 7	55	87	75 ± 8	70	101	84 ± 9
χ_{ARM}/χ	5.15	8.03	6.80 ± 0.53	5.70	8.53	7.55 ± 0.58	7.68	9.37	8.51 ± 0.48
SIRM/χ (kA m^{-1})	8.58	10.00	9.20 ± 0.33	8.96	11.45	10.05 ± 0.52	9.00	11.48	10.23 ± 0.73
S_{-100} (%)	85	88	86 ± 1	83	90	86 ± 1	85	87	86 ± 1
S_{-300} (%)	92	95	93 ± 1	89	98	93 ± 2	92	95	93 ± 1
TOC (%)	0.51	0.87	0.74 ± 0.09	0.59	0.95	0.76 ± 0.09	0.80	0.96	0.87 ± 0.05
C/N	10.63	13.48	11.84 ± 0.60	8.76	12.23	10.99 ± 0.79	9.57	11.39	10.37 ± 0.51
TS (%)	0.04	0.11	0.08 ± 0.02	0.07	0.13	0.10 ± 0.02	0.06	0.17	0.11 ± 0.03
C/S	6.85	18.31	9.92 ± 3.29	5.87	11.28	8.21 ± 1.75	5.32	13.08	8.08 ± 2.01
Mean size (μm)	7	33	15 ± 5	11	39	21 ± 7	8	20	13 ± 3

trend with increasing depth until 170 cm. SIRM generally decreases with depth, with a clear transition zone between 100 cm and 170 cm (Zone B; Figure 4). In Zone C, χ is relatively stable, while χ_{ARM}, χ_{fd}, SIRM, and HIRM decline with increasing depth. Parameter $\chi_{fd\%}$ variations are similar to those of χ_{fd}. S_{-100} and S_{-300} gradually decline downward until 170 cm depth, after which they increase with depth. Stratigraphic trends of χ_{ARM}/χ and χ_{ARM}/SIRM are inversely related to those of the S ratios. SIRM/χ undergoes a more complex pattern of variation, decreasing with depth from 20 cm to 100 cm and then increasing with depth with a broad peak at the boundary of Zones B and C. Subsequently, it decreases again with increasing depth.

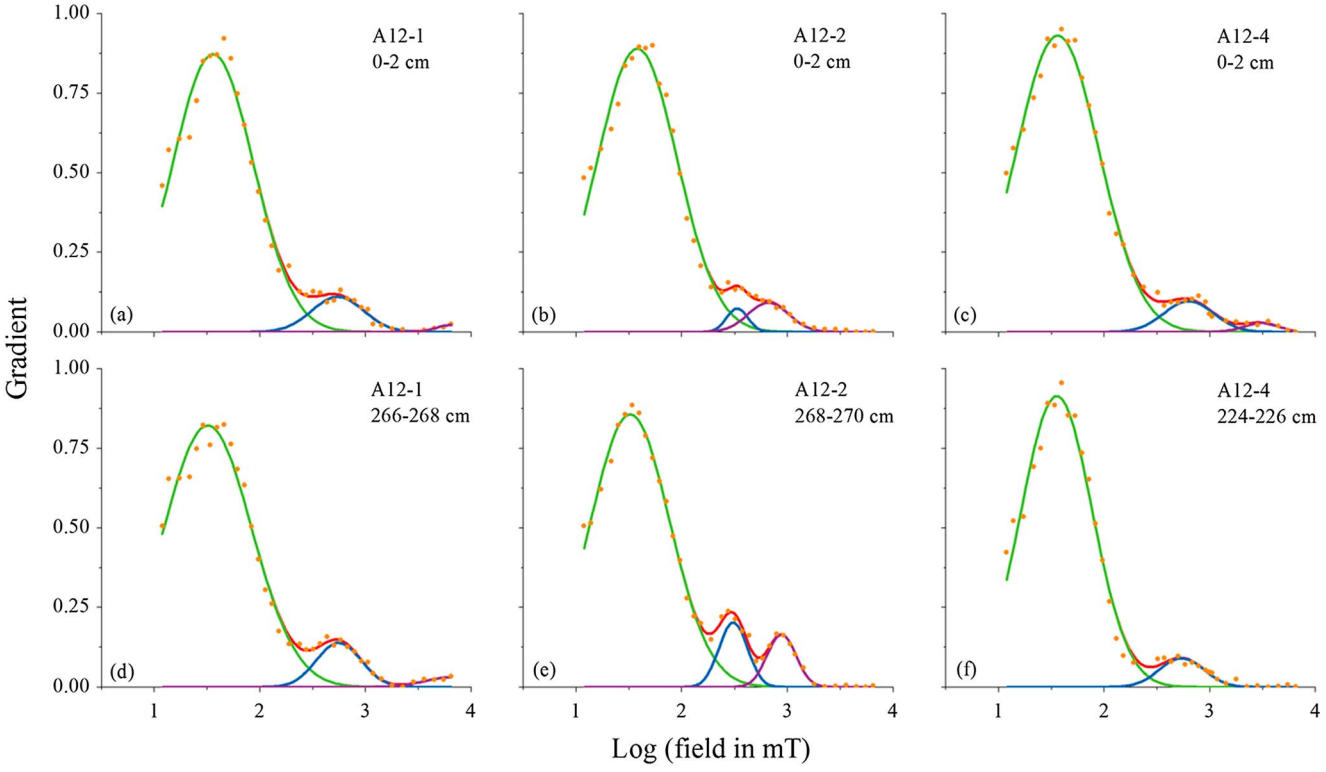

Figure 5. Results of isothermal remanent magnetization (IRM) unmixing analysis [*Kruiver et al.*, 2001] for selected samples. In general, two or three magnetic components are identified.

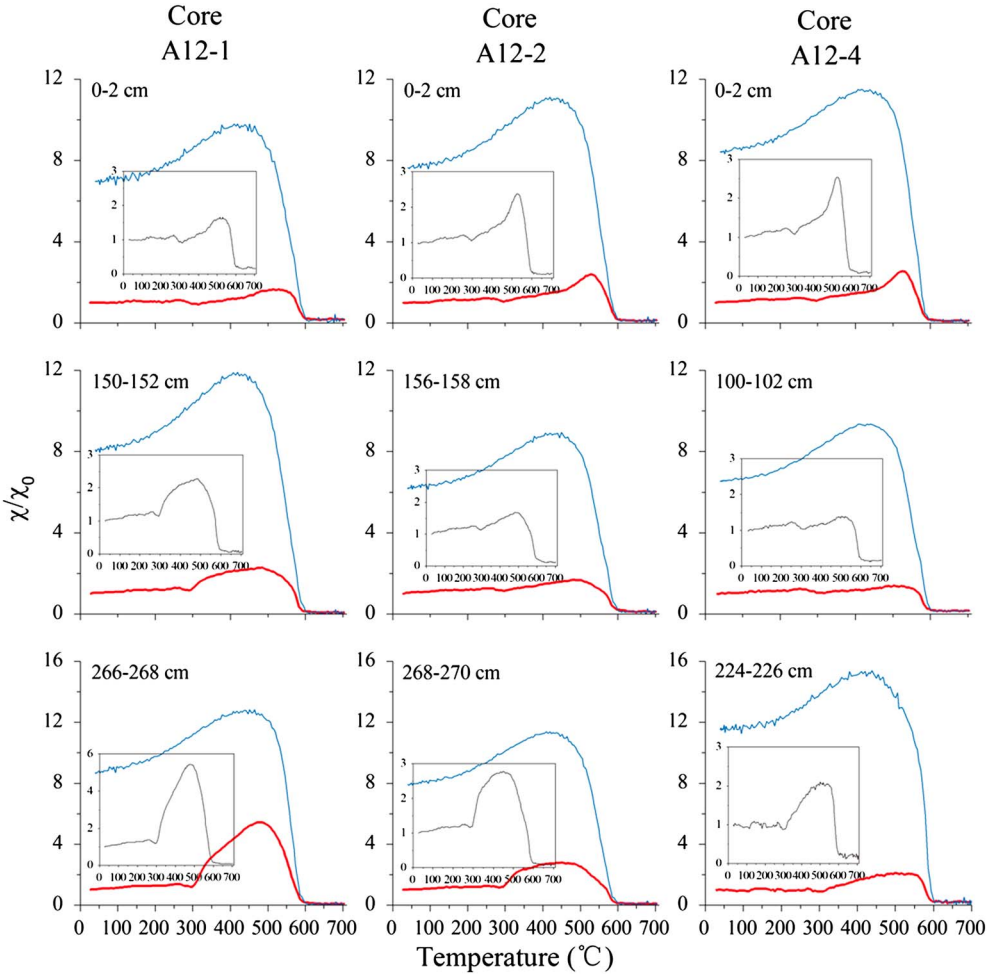

Figure 6. Representative temperature-dependent magnetic susceptibility curves for samples from the studied cores. The red and blue lines represent heating and cooling curves, respectively. The insets include the heating curves only.

3.3.2. IRM Unmixing and Thermomagnetic Analysis

IRM acquisition curves indicate that all of the samples are dominated by a low-coercivity component with a median acquisition field $B_{1/2}$ of ~45 mT, which is typical of magnetite (Figure 5). Medium-coercivity ($B_{1/2}$ of 250–700 mT) and high-coercivity components ($B_{1/2}$ >1000 mT) are also present, which are most likely hematite and goethite, respectively [*Kruiver et al.*, 2001; *Yamazaki and Ikehara*, 2012].

The thermomagnetic curves indicate a Curie temperature of ~580°C; magnetite is therefore the dominant ferrimagnetic mineral (Figure 6) [*Thompson and Oldfield*, 1986], which is consistent with IRM unmixing results (Figure 5). In addition, χ increases gradually with temperature up to 280°C, which is generally due to unblocking of fine grains near the SP/SD boundary [*Liu and Deng*, 2009]. Above 300°C, χ increases and peaks at around 500°C which most likely reflects the transformation of weakly paramagnetic minerals (e.g., iron sulfide, siderite, and clay minerals) to a ferrimagnetic mineral such as magnetite [*Roberts*, 1995; *Maher and Thompson*, 1999; *Pan et al.*, 2000]. Alternatively, it could be caused by conversion of goethite to ferrimagnetic minerals in the presence of organic carbon and calcium carbonate [*Hanesch et al.*, 2006]. The cooling curves all have higher χ values than the heating curves, which is consistent with the formation of ferrimagnetic minerals during heating.

3.4. Carbon, Nitrogen, and Sulfur

In core A12-1, TOC is lower in the upper 80 cm, but it then increases with depth before stabilizing at around 0.75% (Figure 7). TOC in core A12-2 varies slightly, with a mean of 0.75%. In core A12-4, TOC remains uniform

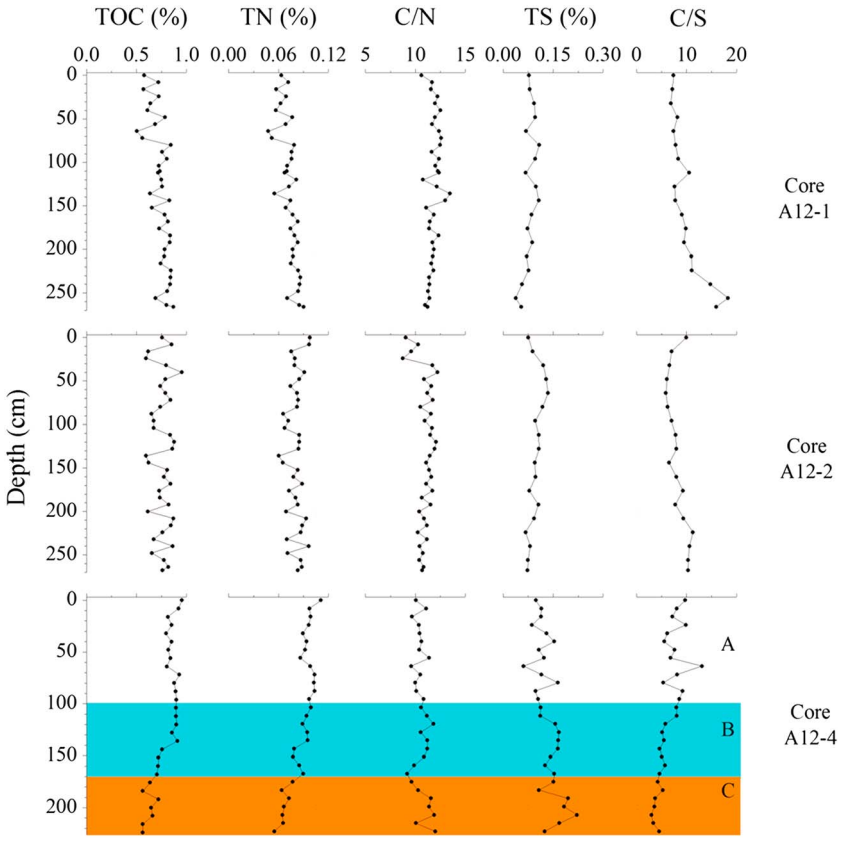

Figure 7. Downcore variations of total organic carbon (TOC), total nitrogen (TN), and total sulfur (TS) and their ratios in cores A12-1, A12-2, and A12-4.

in the upper 150 cm, at around 0.90%, with higher values than the other two cores, and then decreases with depth. These TOC values are similar to those reported previously from the study area [e.g., *Zhu et al*., 2013]. In cores A12-1 and A12-2, the atomic ratio of TOC to TN (C/N) is higher than 10, with lower values at the surface, followed by a subsurface peak, with values then declining downcore. The C/N ratio is relatively stable in core A12-4, with values around 10. In cores A12-1 and A12-2, TS decreases slightly with depth, from 0.08 to 0.04%. In core A12-4, TS is stable in Zone A with values similar to those of the surface samples in cores A12-1 and A12-2 and then increases with depth in Zones B and C. The ratio of TOC to TS (C/S) is stable in the upper part of cores A12-1 and A12-2 and then increases with depth below 200 cm. In core A12-4, the C/S ratio generally decreases with depth.

4. Discussion

4.1. Spatial Variability of Magnetic Properties

Cores A12-1 and A12-2 generally have similar downcore magnetic property variations with a similar range of values (Table 1). Both cores have relatively unvarying profiles of χ, SIRM, χ_{ARM}, χ_{fd}, and HIRM, and the *S* ratios are also relatively stable. The grain size indicators χ_{ARM}/χ and χ_{ARM}/SIRM increase slightly with depth. These characteristics indicate no significant downcore decrease in the concentration of ferrimagnetic minerals; however, there is a slight downcore fining of the ferrimagnetic grain size. Given that the sediments have a common source, i.e., the Yangtze Estuary, this fining trend may be caused by a slight increase in clay content with depth. Notably, a previous study has revealed a significant relationship between clay content and χ_{ARM}/χ and χ_{ARM}/SIRM ratios in surface tidal flat sediments of the Yangtze Estuary [*Zhang and Yu*, 2003]. However, in this study there is only a relatively weak correlation between clay content and magnetic parameters (Table 2), which suggests that factors other than particle size variations are responsible.

Table 2. Pearson's Correlation Coefficients Between Magnetic Parameters and Bulk Sediment Particle Size Fractions[a]

		χ	SIRM	χ_{fd}	χ_{ARM}	HIRM	$\chi_{fd\%}$	χ_{ARM}/SIRM	χ_{ARM}/χ	SIRM/χ	S_{-100}	S_{-300}
A12-1	<4 μm	**0.39**	**0.43**	**0.36**	**0.50**	0.21	0.29	**0.44**	**0.46**	−0.13	0.01	0.04
	4–63 μm	**−0.38**	**−0.41**	**−0.34**	**−0.50**	−0.19	−0.27	**−0.45**	**−0.48**	0.13	−0.01	−0.05
	>63 μm	−0.28	−0.31	−0.29	−0.29	−0.18	−0.24	−0.21	−0.22	0.07	−0.01	0.01
	mean size	**−0.44**	**−0.47**	**−0.40**	**−0.52**	−0.28	**−0.33**	**−0.44**	**−0.45**	0.17	0.00	0.02
A12-2	<4 μm	0.13	−0.12	0.24	0.25	−0.20	0.25	**0.40**	**0.32**	−0.31	−0.04	0.19
	4–63 μm	0.09	0.28	−0.12	−0.05	0.24	−0.17	−0.26	−0.15	0.29	0.03	−0.17
	>63 μm	−0.17	−0.15	0.02	−0.21	−0.20	0.06	−0.16	−0.23	−0.02	0.22	0.17
	mean size	−0.22	−0.09	−0.13	−0.32	−0.08	−0.10	**−0.35**	**−0.37**	0.13	0.22	0.05
A12-4 (0–100 cm)	<4 μm	−0.10	0.03	−0.15	0.30	0.04	−0.13	0.18	0.38	0.07	0.23	−0.02
	4–63 μm	0.13	0.00	0.17	−0.30	−0.06	0.14	−0.21	−0.41	−0.04	−0.16	0.06
	>63 μm	−0.10	−0.13	0.00	−0.10	0.07	0.02	0.05	−0.05	−0.11	−0.33	−0.14
	mean size	0.06	−0.01	0.09	−0.26	0.08	0.08	−0.16	−0.32	−0.03	−0.33	−0.04
A12-4 (100–224 cm)	<4 μm	**0.66**	**0.72**	**0.65**	**0.76**	**0.76**	**0.66**	0.30	0.10	−0.16	**−0.60**	**−0.53**
	4–63 μm	**0.63**	**0.71**	**0.69**	**0.76**	**0.65**	**0.72**	0.36	0.14	−0.18	**−0.47**	−0.31
	>63 μm	**−0.75**	**−0.84**	**−0.79**	**−0.89**	**−0.82**	**−0.81**	−0.39	−0.15	0.20	**0.62**	**0.47**
	mean size	**−0.75**	**−0.83**	**−0.76**	**−0.88**	**−0.80**	**−0.77**	−0.39	−0.15	0.21	**0.57**	**0.46**

[a]The bold type indicates values that are statistically significant at $P < 0.01$.

Core A12-4 can be divided into three zones. The magnetic properties of Zone A are similar to those of cores A12-1 and A12-2 (Figure 4 and Table 1). In Zone B, χ, SIRM, χ_{ARM}, χ_{fd}, and HIRM decline rapidly with increasing depth, while χ_{ARM}/χ and χ_{ARM}/SIRM increase with depth. *S* ratios decline with depth in this zone, while SIRM/χ increases. In Zone C, χ, SIRM, χ_{ARM}, χ_{fd}, and HIRM generally remain stable or decline with depth. Parameters χ_{ARM}/χ, χ_{ARM}/SIRM, and SIRM/χ decline with depth, while *S* ratios increase. Core F17 (Figure 1), which was recovered southwestern to the transect (water depth 41.4 m and sedimentation rate ~0.49 cm/yr) [*Hu et al*., 2012], has a similar downcore pattern of magnetic variability to core A12-4. Although changes in the particle size distribution of bulk sediment may be responsible for changes in concentration-related magnetic properties, no significant relationships are observed between χ_{ARM}/χ, χ_{ARM}/SIRM, and sediment particle size (Table 2). This can be demonstrated by opposite trends of ferrimagnetic grain size indicators and mean sediment particle size in Zone B, assuming that coarser sediments would normally contain coarser ferrimagnetic grains [*Oldfield et al*., 1985, 2009]. This suggests that variations in bulk sediment particle size alone cannot fully explain the downcore magnetic property variations.

Stratigraphic variations of magnetic properties of core A12-4 are consistent with progressive magnetic mineral diagenesis, as observed elsewhere in marine and coastal sediments [*Zheng et al*., 2010, 2011; *Mohamed et al*., 2011]. Usually, Zone A is a suboxic zone characterized by weakly reducing conditions. Iron oxides with reactivity greater than magnetite (e.g., ferrihydrite) are removed first [*Poulton et al*., 2004], and therefore, χ remains largely unaffected. In this respect, the whole of cores A12-1 and A12-2 are magnetically equivalent to Zone A of core A12-4, as supported by statistical analysis of the magnetic properties of cores A12-1 and A12-2 and the upper 100 cm of A12-4, which have similar values for the range and mean of magnetic parameters (Table 1). Despite the different downcore trends in clay content variation (Figure 2), the common pattern of ferrimagnetic particle fining with depth in cores A12-1 and A12-2, and in the upper 100 cm of core A12-4, further indicates that factors other than variations in bulk sediment particle size are responsible. Zone B is characterized by intense sulfate reduction and abundant iron sulfide precipitation [*Mohamed et al*., 2011]. The occurrence of these processes in the studied sediments is supported by the increased TS contents. Hence, rapid magnetite dissolution and, thus, decreasing magnetite concentration have occurred with increasing depth in this zone. Imperfect antiferromagnetic minerals are more resistant to reductive dissolution than magnetite [*Yamazaki et al*., 2003; *Emiroğlu et al*., 2004; *Liu et al*., 2004; *Rey et al*., 2005; *Kawamura et al*., 2007; *Rowan et al*., 2009; *Mohamed et al*., 2011], which has resulted in a downcore decrease in *S* ratios. With increasing depth in Zone C, both reactive magnetite and imperfect antiferromagnetic minerals are removed and χ is further reduced to uniformly low values.

Although χ is relatively stable in Zone A, a common feature is a downward fining trend of ferrimagnetic grain size as suggested by stratigraphic variations of χ_{ARM}/χ, χ_{ARM}/SIRM, and $\chi_{fd\%}$; i.e., the proportions of SP and SD

grains increase with depth. The decreasing SIRM/χ trend with depth can be explained by an increasing proportion of SP grains with depth. This downward increasing trend of χ_{ARM}/χ and χ_{ARM}/SIRM extends to Zone B; however, SIRM/χ then reverts, which can be explained by a lower SP contribution to χ in Zone B. By comparison, the proportion of SD grains continues to increase in Zone B. This feature has previously been observed in the study area [*Zheng et al*., 2011; *Hu et al*., 2012] and is explained by an increase in the proportion of the ferrimagnetic iron sulfide greigite, as confirmed by scanning electron microscope observations [*Hu et al*., 2012]. Similar phenomena have been documented from the Ria de Vigo [*Mohamed et al*., 2011] and deeper water continental margin settings [*Rowan et al*., 2009]. It is well known that greigite forms near the boundary between iron-reducing and sulfate-reducing conditions, where the combination of reducing conditions and limited HS^- accumulation favors greigite preservation [*Kao et al*., 2004]. In a geochemical study of sediment core C702, close to the study area (Figure 1), pore water sulfide was not detected (<1 μmol/g) in the upper 40 cm of sediment [*Zhu et al*., 2013]. Acid volatile sulfide begins to increase at a depth of 10 cm in core C702, where values of 3–6 μmol/g are observed. By comparison, the elemental sulfur content is much lower (0–1 μmol/g). The high reactive iron supply in relation to the relatively low sulfide concentration favors greigite formation and preservation [cf. *Kao et al*., 2004]. Using a geochemical sequential extraction method, *Lü et al*. [2011] reported a higher abundance of greigite within iron sulfide assemblages in core 0701 in a nearby region (Figure 1). The neoformed greigite can be SP or SD in size [*Rowan and Roberts*, 2006; *Rowan et al*., 2009], which results in a fining of ferrimagnetic grain size with increasing depth. In Zone B, with increasingly reducing conditions, detrital SP grains are removed first, followed by SD grains, which leads to a coarsening of the detrital ferrimagnetic grain size distribution in Zone C, as reflected by lower χ_{ARM}/χ and χ_{ARM}/SIRM values.

4.2. Influence of Organic Matter and Sedimentation Rate on Magnetic Mineral Diagenesis

Several studies have documented the magnetic and sedimentological properties of the transition between Zones A and B, where χ starts to decrease. In the Okhotsk Sea, this boundary is located at sediment depths shallower than 80 cm except for one site where it occurs 130 cm below the seafloor [*Kawamura et al*., 2007]. In the biologically productive Ria de Vigo Estuary, the maximum depth of this boundary is 40 cm [*Mohamed et al*., 2011]. In core A12-4, the transition occurs at 100 cm depth. TOC has been invoked to explain the spatial variation of the transition from Zone A to Zone B in the Ria de Vigo, with higher TOC values leading to a shallower depth of this transition zone [*Mohamed et al*., 2011]. Thus, it seems that TOC may explain the depth variation of this transition in different coastal seas of the world. The studied cores have TOC values less than 1%, which is much lower than that of the sites mentioned above (>1%). Core A12-4 has higher TOC and a shallow transition depth, which is consistent with previous observations [*Mohamed et al*., 2011].

In addition to sedimentary TOC, the reactivity of organic carbon has an important influence on the rate of reductive diagenesis. The coastal waters in the study area have a high sediment load, and a significant proportion of the sedimentary organic matter (up to 54%) is of terrestrial origin [*Li et al*., 2013]. In addition, physical reworking of sediments by currents and wave activity in the shallower margins would increase sediment oxygenation and enhance carbon remineralization [*Aller et al*., 1985; *DeMaster et al*., 1985]. It has been found that sediment in the study area has a relatively low ratio of TOC to sediment surface area (<0.40 mg/m^2) [*Blair and Aller*, 2012; *Wu et al*., 2013; *Yao et al*., 2014], which would lead to refractory carbon being deposited in the sediments [*Blair and Aller*, 2012]. The lower reactivity of organic carbon, combined with higher reactive iron oxide content, is likely to have led to a lower sulfate reduction rate. The almost homogeneous TOC of cores A12-1 and A12-2 also suggests that postdepositional organic carbon degradation is limited. In core A12-4, TOC is generally higher than in the two other cores. The slightly lower C/N ratio of core A12-4 implies a higher proportion of marine carbon, which is consistent with the observed decreasing proportion of terrestrial organic carbon offshore, as indicated by organic geochemical characterization [*Li et al*., 2013]. Marine organic carbon is considered to be more reactive than terrestrial carbon [*Burdige*, 2005]. TOC starts to decrease in the middle part of Zone B, which suggests that significant magnetite dissolution is linked to organic carbon degradation (Figure 7).

Sedimentation rate has also been suggested to have an influence on magnetic mineral diagenesis [e.g., *Zheng et al*., 2011]. The incomplete magnetic zonation of cores A12-1 and A12-2, i.e., the absence of a zone of rapidly declining concentration-dependent magnetic parameters (e.g., χ), followed by a stable zone,

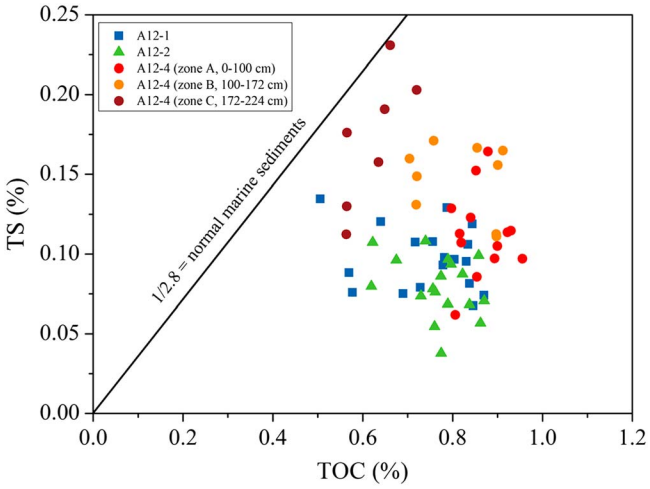

Figure 8. Scatterplot of total sulfur (TS) versus total organic carbon (TOC) for the studied sediments. The line that indicates a TS/TOC ratio of 1/2.8 represents the value for normal marine sediments [*Berner*, 1982] and is included for reference.

could be due to the fact that these cores have much higher sedimentation rates than core A12-4. Thus, cores A12-1 and A12-2 are not long enough to have reached Zones B and C, which are present in core A12-4. Therefore, in the study area, this transitional boundary can be at least 250 cm below the sediment surface where the sedimentation rate is greater than ~1 cm/yr (the sedimentation rate for core A12-2). Several explanations can be offered. Rapid sedimentation rates will limit delivery of dissolved sulfate from the overlying water to the sediments [*Hedges and Keil*, 1995]. Abundant supply of iron oxides to accumulating sediments will also suppress sulfate reduction [*Kao et al*., 2004]. The influence of sedimentation rate is an indirect one, and its impact on organic carbon decomposition is dependent on the resulting flux of organic carbon and its reactivity [*Arndt et al*., 2013]. Higher sedimentation rates in the inner sites lead to less labile marine organic carbon delivery to the sediments as mentioned earlier. In such a case, higher sedimentation rates will result in a deeper iron- to sulfate-reduction transition boundary.

4.3. Implications of the Results for the Iron-Sulfur Cycle in Continental Shelf Sediments

Since the iron cycle in continental shelf sediments is closely linked to biological productivity in the water column, carbon burial, and the fate of pollutants, there have been extensive studies of iron diagenesis and its coupling with carbon and sulfur [*Kao et al*., 2004; *Zhu et al*., 2013]. These studies have focused on the relative importance of iron reduction versus sulfate reduction in organic carbon mineralization, which is related to the lability of buried organic carbon, the availability of pore water sulfate, and the abundance of reactive iron oxides. In this study, the deeper location of ISRB, as inferred from the magnetic mineral zonation, implies that ferruginous diagenesis is more important than sulfate reduction in the river-dominated inner shelf of the East China Sea. The lower TS/TOC ratio (Figure 8), which is generally less than the value of 1/2.8 for typical marine sediments, also implies a low degree of pyritization compared to other marine and coastal environments [*Berner*, 1982]. Previous geochemical studies have suggested that sulfate reduction is less important in organic matter degradation in the East China Sea due to a higher proportion of refractory terrestrial organic matter, abundant reactive iron oxides, and the physical reworking of sediments [*Kao et al*., 2004; *Zhu et al*., 2013]. Therefore, we suggest that analysis of magnetic mineral diagenetic zonations provides a straightforward approach to assess organic carbon decomposition pathways, with deeper ISRB depth reflecting relatively limited sulfate reduction.

5. Conclusions

A combination of magnetic measurements, geochemical analyses, and radionuclide dating reveals significant spatial variability of magnetic mineral diagenesis in river-dominated inner shelf deposits in the East China Sea. In this environment, the sedimentation rate and proportion of terrestrial organic matter decrease from onshore to offshore. The magnetic properties of the studied cores are spatially variable, with the cores nearest shore undergoing less reductive magnetite dissolution and having a much deeper transition from iron to sulfate reduction than the seaward cores. Compared to more typical marine environments and sediment-starved coastal areas, the study area has a much higher modern sedimentation rate, lower sedimentary TOC, and a deeper transition from iron- to sulfate-reduction conditions. In view of the rich supply of iron oxides and refractory organic carbon to the studied sediments, as confirmed by previous

geochemical studies, we suggest that sulfidic diagenesis in rapidly accumulating river-dominated margins has less influence on sedimentary magnetic properties compared to more typical marine environments. Finally, the use of stratigraphic zonation of magnetic mineral diagenesis constitutes a simple approach for assessing the relative importance of iron and sulfate reduction associated with organic carbon oxidation in marine sediments.

Acknowledgments

The data presented in this paper are available at the Information Center of the State Key Laboratory of Estuarine and Coastal Research, East China Normal University. Qing Yuan (qyuan@sklec.ecnu.edu.cn) can be contacted for access to the data. This study was supported in part by the National Natural Science Foundation of China (40771201 and 41202243), the Ministry of Science and Technology fundamental project (2013FY112000), and the State Key Laboratory Special Fund of China (2012KYYW01). We thank Jan Bloemendal, Andrew P. Roberts, and an anonymous reviewer for their constructive comments and language improvement. We appreciate Honghua Lü and Peiqin Wang for their cartographic assistance.

References

Aller, R. C., J. E. Mackin, W. J. Ullman, C. H. Wang, S. M. Tsai, J. C. Jin, Y. N. Sui, and J. Z. Hong (1985), Early chemical diagenesis, sediment-water solute exchange, and storage of reactive organic matter near the mouth of the Changjiang, East China Sea, *Cont. Shelf Res.*, *4*, 227–251, doi:10.1016/0278-4343(85)90031-7.

Appleby, P. G., and F. Oldfield (1978), The calculation of lead-210 dates assuming a constant rate of supply of unsupported ^{210}Pb to the sediment, *Catena*, *5*, 1–8, doi:10.1016/S0341-8162(78)80002-2.

Arndt, S., B. B. Jørgensen, D. E. LaRowe, J. J. Middelburg, R. D. Pancost, and P. Regnier (2013), Quantifying the degradation of organic matter in marine sediments: A review and synthesis, *Earth Sci. Rev.*, *123*, 53–86, doi:10.1016/j.earscirev.2013.02.008.

Banerjee, S. K., J. King, and J. Marvin (1981), A rapid method for magnetic granulometry with applications to environmental studies, *Geophys. Res. Lett.*, *8*, 333–336, doi:10.1029/GL008i004p00333.

Berner, R. A. (1982), Burial of organic carbon and pyrite sulfur in the modern ocean: Its geochemical and environmental significance, *Am. J. Sci.*, *282*, 451–473, doi:10.2475/ajs.282.4.451.

Blair, N. E., and R. C. Aller (2012), The fate of terrestrial organic carbon in the marine environment, *Annu. Rev. Mar. Sci.*, *4*, 401–423, doi:10.1146/annurev-marine-120709-142717.

Blanchet, C. L., N. Thouveny, and L. Vidal (2009), Formation and preservation of greigite (Fe_3S_4) in sediments from the Santa Barbara Basin: Implications for paleoenvironmental changes during the past 35 ka, *Paleoceanography*, *24*, PA2224, doi:10.1029/2008PA001719.

Bloemendal, J., and X. M. Liu (2005), Rock magnetism and geochemistry of two Plio-Pleistocene Chinese loess-palaeosol sequences—Implications for quantitative palaeoprecipitation reconstruction, *Palaeogeogr. Palaeoclimatol. Palaeoecol.*, *226*, 149–166, doi:10.1016/j.palaeo.2005.05.008.

Bloemendal, J., J. W. King, F. R. Hall, and S. J. Doh (1992), Rock magnetism of Late Neogene and Pleistocene deep-sea sediments: Relationship to sediment source, diagenetic processes, and sediment lithology, *J. Geophys. Res.*, *97*, 4361–4375, doi:10.1029/91JB03068.

Bouilloux, A., J. P. Valet, F. Bassinot, J. L. Joron, M. M. Blanc Valleron, E. Moreno, F. Dewilde, M. Kars, and F. Lagroix (2013), Diagenetic modulation of the magnetic properties in sediments from the Northern Indian Ocean, *Geochem. Geophys. Geosyst.*, *14*, 3779–3800, doi:10.1002/ggge.20234.

Burdige, D. J. (1993), The biogeochemistry of manganese and iron reduction in marine sediments, *Earth Sci. Rev.*, *35*, 249–284, doi:10.1016/0012-8252(93)90040-E.

Burdige, D. J. (2005), Burial of terrestrial organic matter in marine sediments: A re-assessment, *Global Biogeochem. Cycles*, *19*, GB4011, doi:10.1029/2004GB002368.

Canfield, D. E., and R. A. Berner (1987), Dissolution and pyritization of magnetite in anoxic marine sediments, *Geochim. Cosmochim. Acta*, *51*, 645–659, doi:10.1016/0016-7037(87)90076-7.

Chen, Z. Y., Y. Saito, Y. Kanai, T. Y. Wei, L. Q. Li, H. S. Yao, and Z. H. Wang (2004), Low concentration of heavy metals in the Yangtze estuarine sediments, China: A diluting setting, *Estuarine Coastal Shelf Sci.*, *60*, 91–100, doi:10.1016/j.ecss.2003.11.021.

DeMaster, D. J., B. A. McKee, C. A. Nittrouer, J. C. Qian, and G. D. Cheng (1985), Rates of sediment accumulation and particle reworking based on radiochemical measurements from continental shelf deposits in the East China Sea, *Cont. Shelf Res.*, *4*, 143–158, doi:10.1016/0278-4343(85)90026-3.

Emiroğlu, S., D. Rey, and N. Petersen (2004), Magnetic properties of sediment in the Ria de Arousa (Spain): Dissolution of iron oxides and formation of iron sulphides, *Phys. Chem. Earth*, *29*, 947–959, doi:10.1016/j.pce.2004.03.012.

Fu, Y. Z., T. von Dobeneck, C. Franke, D. Heslop, and S. Kasten (2008), Rock magnetic identification and geochemical process models of greigite formation in Quaternary marine sediments from the Gulf of Mexico (IODP Hole U1319A), *Earth Planet. Sci. Lett.*, *275*, 233–245, doi:10.1016/j.epsl.2008.07.034.

Hanesch, M., H. Stanjek, and N. Petersen (2006), Thermomagnetic measurements of soil iron minerals: The role of organic carbon, *Geophys. J. Int.*, *165*, 53–61, doi:10.1111/j.1365-246X.2006.02933.x.

Hedges, J. I., and R. G. Keil (1995), Sedimentary organic matter preservation: An assessment and speculative synthesis, *Mar. Chem.*, *49*, 81–115, doi:10.1016/0304-4203(95)00008-F.

Horng, C., C. Laj, T. Lee, and J. Chen (1992), Magnetic characteristics of sedimentary rocks from the Tsengwen-chi and Erhjen-chi sections in southwestern Taiwan, *TAO*, *3*, 519–532.

Hu, Z. X., W. G. Zhang, C. Y. Dong, Y. Liu, J. Chen, and L. Z. Yu (2012), Influence of early diagenesis on magnetic properties of inner shelf deposits of the East China Sea [in Chinese with English abstract], *Quat. Sci.*, *32*, 670–678, doi:10.3969/j.issn.1001-7410.2012.04.12.

Huh, C. A., and C. C. Su (1999), Sedimentation dynamics in the East China Sea elucidated from ^{210}Pb, ^{137}Cs and ^{239,240}Pu, *Mar. Geol.*, *160*, 183–196, doi:10.1016/S0025-3227(99)00020-1.

Kao, S. J., C. S. Horng, A. P. Roberts, and K. K. Liu (2004), Carbon-sulfur-iron relationships in sedimentary rocks from southwestern Taiwan: Influence of geochemical environment on greigite and pyrrhotite formation, *Chem. Geol.*, *203*, 153–168, doi:10.1016/j.chemgeo.2003.09.007.

Karlin, R. (1990), Magnetite diagenesis in marine sediments from the Oregon continental margin, *J. Geophys. Res.*, *95*, 4405–4419, doi:10.1029/JB095iB04p04405.

Karlin, R., and S. Levi (1983), Diagenesis of magnetic minerals in recent haemipelagic sediments, *Nature*, *303*, 327–330, doi:10.1038/303327a0.

Kawamura, N., H. Oda, K. Ikehara, T. Yamazaki, K. Shioi, S. Taga, S. Hatakeyama, and M. Torii (2007), Diagenetic effect on magnetic properties of marine core sediments from the southern Okhotsk Sea, *Earth Planets Space*, *59*, 83–93, doi:10.1186/BF03352680.

Kruiver, P. P., M. J. Dekkers, and D. Heslop (2001), Quantification of magnetic coercivity components by the analysis of acquisition curves of isothermal remanent magnetization, *Earth Planet. Sci. Lett.*, *189*, 269–276, doi:10.1016/S0012-821X(01)00367-3.

Li, X. X., T. S. Bianchi, and M. A. Allison (2013), Historical reconstruction of organic carbon decay and preservation in sediments on the East China Sea shelf, *J. Geophys. Res. Biogeosci.*, *118*, 1079–1093, doi:10.1002/jgrg.20079.

Liu, J., R. Zhu, A. P. Roberts, S. Li, and J. H. Chang (2004), High-resolution analysis of early diagenetic effects on magnetic minerals in post-middle-Holocene continental shelf sediments from the Korea Strait, *J. Geophys. Res.*, *109*, B03103, doi:10.1029/2003JB002813.

Liu, J. P., K. H. Xu, A. C. Li, J. D. Milliman, D. M. Velozzi, S. B. Xiao, and Z. S. Yang (2007), Flux and fate of Yangtze River sediment delivered to the East China Sea, *Geomorphology*, *85*, 208–224, doi:10.1016/j.geomorph.2006.03.023.

Liu, Q., A. P. Roberts, J. C. Larrasoaña, S. K. Banerjee, Y. Guyodo, L. Tauxe, and F. Oldfield (2012), Environmental magnetism: Principles and applications, *Rev. Geophys.*, *50*, RG4002, doi:10.1029/2012RG000393.

Liu, Q. S., and C. L. Deng (2009), Magnetic susceptibility and its environmental significances [in Chinese with English abstract], *Chin. J. Geophys.*, *52*, 1041–1048.

Lu, R. K. (2000), *Soil and Agricultural Chemistry Analysis Method* [in Chinese], China Agricultural Science and Technology Press, Beijing.

Lü, R. Y., M. X. Zhu, J. P. Yang, and F. F. Deng (2011), Speciation of solid-phase iron in mud sediments collected from the shelf of the East China Sea: Constraints on diagenetic pathways of organic matter, iron, and sulfur [in Chinese with English abstract], *Geochimica*, *40*, 363–371.

Maher, B. A. (1988), Magnetic properties of some synthetic sub-micron magnetites, *Geophys. J. Int.*, *94*, 83–96, doi:10.1111/j.1365-246X.1988.tb03429.x.

Maher, B. A., and R. Thompson (1999), *Quaternary Climates, Environments and Magnetism*, Cambridge Univ. Press, Cambridge, U. K.

Milliman, J. D., H. T. Shen, Z. S. Yang, and H. M. Robert (1985), Transport and deposition of river sediment in the Changjiang estuary and adjacent continental shelf, *Cont. Shelf Res.*, *4*, 37–45, doi:10.1016/0278-4343(85)90020-2.

Mohamed, K. J., D. Rey, B. Rubio, M. J. Dekkers, A. P. Roberts, and F. Vilas (2011), Onshore-offshore gradient in reductive early diagenesis in coastal marine sediments of the Ria de Vigo, Northwest Iberian Peninsula, *Cont. Shelf Res.*, *31*, 433–447, doi:10.1016/j.csr.2010.06.006.

Oldfield, F. (1994), Toward the discrimination of fine-grained ferrimagnets by magnetic measurements in lake and near-shore marine sediments, *J. Geophys. Res.*, *99*, 9045–9050, doi:10.1029/93JB03137.

Oldfield, F., B. A. Maher, J. Donoghue, and J. Pierce (1985), Particle-size related, mineral magnetic source sediment linkages in the Rhode River catchment, Maryland, USA, *J. Geol. Soc. London*, *142*, 1035–1046, doi:10.1144/gsjgs.142.6.1035.

Oldfield, F., Q. Z. Hao, J. Bloemendal, Z. Gibbs Eggar, S. Patil, and Z. T. Guo (2009), Links between bulk sediment particle size and magnetic grain-size: General observations and implications for Chinese loess studies, *Sedimentology*, *56*, 2091–2106, doi:10.1111/j.1365-3091.2009.01071.x.

Pan, S. M., S. G. Tims, X. Y. Liu, and L. K. Fifield (2011), ^{137}Cs, $^{239+240}$Pu concentrations and the ^{240}Pu/^{239}Pu atom ratio in a sediment core from the sub-aqueous delta of Yangtze River estuary, *J. Environ. Radioact.*, *102*, 930–936, doi:10.1016/j.jenvrad.2010.05.012.

Pan, Y. X., R. X. Zhu, S. K. Banerjee, J. Gill, and Q. Williams (2000), Rock magnetic properties related to thermal treatment of siderite: Behavior and interpretation, *J. Geophys. Res.*, *105*(B1), 783–794, doi:10.1029/1999JB900358.

Poulton, S. W., M. D. Krom, and R. Raiswell (2004), A revised scheme for the reactivity of iron (oxyhydr) oxide minerals towards dissolved sulfide, *Geochim. Cosmochim. Acta*, *68*, 3703–3715, doi:10.1016/j.gca.2004.03.012.

Qin, Y. S., Y. Y. Zhao, L. R. Chen, and S. L. Zhao (1987), *Geology of the East China Sea* [in Chinese], China Science Press, Beijing.

Rey, D., K. J. Mohamed, A. Bernabeu, B. Rubio, and F. Vilas (2005), Early diagenesis of magnetic minerals in marine transitional environments: Geochemical signatures of hydrodynamic forcing, *Mar. Geol.*, *215*, 215–236, doi:10.1016/j.margeo.2004.12.001.

Roberts, A. P. (1995), Magnetic properties of sedimentary greigite (Fe_3S_4), *Earth Planet. Sci. Lett.*, *134*, 227–236, doi:10.1016/0012-821X(95)00131-U.

Roberts, A. P., and G. M. Turner (1993), Diagenetic formation of ferrimagnetic iron sulphide minerals in rapidly deposited marine sediments, South Island, New Zealand, *Earth Planet. Sci. Lett.*, *115*, 257–273, doi:10.1016/0012-821X(93)90226-Y.

Roberts, A. P., F. Florindo, L. Chang, D. Heslop, L. Jovane, and J. C. Larrasoaña (2013), Magnetic properties of pelagic marine carbonates, *Earth Sci. Rev.*, *127*, 111–139, doi:10.1016/j.earscirev.2013.09.009.

Robinson, S. G., J. T. S. Sahota, and F. Oldfield (2000), Early diagenesis in North Atlantic abyssal plain sediments characterized by rock-magnetic and geochemical indices, *Mar. Geol.*, *163*, 77–107, doi:10.1016/S0025-3227(99)00108-5.

Rowan, C. J., and A. P. Roberts (2006), Magnetite dissolution, diachronous greigite formation, and secondary magnetizations from pyrite oxidation: Unravelling complex magnetizations in Neogene marine sediments from New Zealand, *Earth Planet. Sci. Lett.*, *241*, 119–137, doi:10.1016/j.epsl.2005.10.017.

Rowan, C. J., A. P. Roberts, and T. Broadbent (2009), Reductive diagenesis, magnetite dissolution, greigite growth and paleomagnetic smoothing in marine sediments: A new view, *Earth Planet. Sci. Lett.*, *277*, 223–235, doi:10.1016/j.epsl.2008.10.016.

Shan, X. Q., B. Chen, J. Tie, G. G. Xie, Y. Zheng, and L. Z. Jin (1991), Fractionation of sulphur in soil and river sediment [in Chinese with English abstract], *Acta Scien. Circum.*, *11*, 172–177.

Thompson, R., and F. Oldfield (1986), *Environmental Magnetism*, Allen and Unwin, London.

Tric, E., C. Laj, C. Jéhanno, J. Valet, C. Kissel, A. Mazaud, and S. Iaccarino (1991), High-resolution record of the Upper Olduvai transition from Po Valley (Italy) sediments: Support for dipolar transition geometry?, *Phys. Earth Planet. Inter.*, *65*, 319–336, doi:10.1016/0031-9201(91)90138-8.

Wu, Y., T. Eglinton, L. Yang, B. Deng, D. Montluçon, and J. Zhang (2013), Spatial variability in the abundance, composition, and age of organic matter in surficial sediments of the East China Sea, *J. Geophys. Res. Biogeosci.*, *118*, 1495–1507, doi:10.1002/2013JG002286.

Yamazaki, T. (2009), Environmental magnetism of Pleistocene sediments in the North Pacific and Ontong-Java Plateau: Temporal variations of detrital and biogenic components, *Geochem. Geophys. Geosyst.*, *10*, Q07Z04, doi:10.1029/2009GC002413.

Yamazaki, T., and M. Ikehara (2012), Origin of magnetic mineral concentration variation in the Southern Ocean, *Paleoceanography*, *27*, PA2206, doi:10.1029/2011PA002271.

Yamazaki, T., A. L. Abdeldayem, and K. Ikehara (2003), Rock-magnetic changes with reduction diagenesis in Japan Sea sediments and preservation of geomagnetic secular variation in inclination during the last 30,000 years, *Earth Planets Space*, *55*, 327–340, doi:10.1186/BF03351766.

Yao, P., B. Zhao, T. S. Bianchi, Z. G. Guo, M. X. Zhao, D. Li, H. H. Pan, J. P. Wang, T. T. Zhang, and Z. G. Yu (2014), Remineralization of sedimentary organic carbon in mud deposits of the Changjiang Estuary and adjacent shelf: Implications for carbon preservation and authigenic mineral formation, *Cont. Shelf Res.*, *91*, 1–11, doi:10.1016/j.csr.2014.08.010.

Zhang, W. G., and L. Z. Yu (2003), Magnetic properties of tidal flat sediments of the Yangtze Estuary and its relationship with particle size, *Sci. China, Ser. D: Earth Sci.*, *46*, 954–966, doi:10.1007/BF02991341.

Zheng, Y., C. Kissel, H. B. Zheng, C. Laj, and K. Wang (2010), Sedimentation on the inner shelf of the East China Sea: Magnetic properties, diagenesis and paleoclimate implications, *Mar. Geol.*, *268*, 34–42, doi:10.1016/j.margeo.2009.10.009.

Zheng, Y., H. B. Zheng, C. Kissel, and C. Laj (2011), Sedimentation rate control on diagenesis, East China Sea sediments, *Phys. Earth Planet. Inter.*, *187*, 301–309, doi:10.1016/j.pepi.2011.05.005.

Zhu, M. X., X. N. Shi, G. P. Yang, and X. C. Hao (2013), Formation and burial of pyrite and organic sulfur in mud sediments of the East China Sea inner shelf: Constraints from solid-phase sulfur speciation and stable sulfur isotope, *Cont. Shelf Res.*, *54*, 24–36, doi:10.1016/j.csr.2013.01.002.